# Determination of the resistivity anisotropy of orthorhombic materials via transverse resistivity measurements

P. Walmsley and I. R. Fisher

Citation: Review of Scientific Instruments **88**, 043901 (2017); doi: 10.1063/1.4978908
View online: http://dx.doi.org/10.1063/1.4978908
View Table of Contents: http://aip.scitation.org/toc/rsi/88/4
Published by the American Institute of Physics

# Determination of the resistivity anisotropy of orthorhombic materials via transverse resistivity measurements

P. Walmsley[1,2,a] and I. R. Fisher[1,2]
[1]*Geballe Laboratory for Advanced Materials and Department of Applied Physics, Stanford University, Stanford, California 94305-4045, USA*
[2]*Stanford Institute for Materials and Energy Sciences, SLAC National Accelerator Laboratory, 2575 Sand Hill Road, Menlo Park, California 94025, USA*

(Received 7 October 2016; accepted 7 March 2017; published online 5 April 2017)

Measurements of the resistivity anisotropy can provide crucial information about the electronic structure and scattering processes in anisotropic and low-dimensional materials, but quantitative measurements by conventional means often suffer very significant systematic errors. Here we describe a novel approach to measuring the resistivity anisotropy of orthorhombic materials, using a single crystal and a single measurement that is derived from a $\frac{\pi}{4}$ rotation of the measurement frame relative to the crystallographic axes. In this new basis, the transverse resistivity gives a direct measurement of the resistivity anisotropy, which combined with the longitudinal resistivity also gives the in-plane elements of the conventional resistivity tensor via a 5-point contact geometry. This is demonstrated through application to the charge-density wave compound $ErTe_3$, and it is concluded that this method presents a significant improvement on existing techniques, particularly when measuring small anisotropies. *Published by AIP Publishing.* [http://dx.doi.org/10.1063/1.4978908]

## I. INTRODUCTION

Electrical transport measurements have long been a cornerstone of condensed matter physics as they are necessarily sensitive to the Fermi surface and interactions that are close in energy to the Fermi level. For example, it is often the case that phase transitions in conducting materials are observable as a sharp feature or change in slope of the temperature dependence of the resistivity. By extension, anisotropies in electrical transport can reflect the presence of broken rotational symmetries, and their measurement can contribute to understanding the nature and origin of associated phase transitions, particularly those that are driven by interactions at the Fermi-level. For example, in the case of an electronic nematic phase transition,[1,2] close to the critical temperature the resistivity anisotropy is proportional to the nematic order parameter,[3–6] motivating measurement of the resistivity anisotropy for detwinned samples. The Fe-based superconductors provide a recent example of such an effect. For several families of Fe-based materials, the measurement of the resistivity anisotropy in the broken symmetry state[7–16] and also the measurement of the strain-induced resistivity anisotropy (elastoresistivity) in the tetragonal state[17–22] have provided evidence that the tetragonal-to-orthorhombic phase transition that occurs in many of these materials is indeed driven by electronic correlations; a conclusion supported by Raman spectroscopy[23] and shear modulus measurements.[24] Distinct from the previous example are the materials that are fundamentally orthorhombic even at high temperatures, but which nevertheless develop an enhanced electronic anisotropy below some characteristic temperature. In these cases, changes in the resistivity anisotropy can still reveal important information regarding the origin of the associated phase transition or crossover, also motivating the measurement of the temperature dependence of the resistivity anisotropy. A well-known example is that of the cuprate superconductor $YBa_2Cu_3O_{7-\delta}$, where the presence of CuO chains leads to a fundamentally orthorhombic crystal structure, yet for which several measurements indicate the onset of an enhancement in the electronic anisotropy below a characteristic temperature.[25–28] This additional anisotropy has been discussed in terms of an onset of nematicity that may be connected to the fluctuations of spin-density wave and charge-density wave (CDW) ordering observed in this material.[26,29,30] A second example in this latter class for which the physical origin is much clearer is the quasi 2-D material $RTe_3$ (where $R$ is a rare-earth ion). This material is also orthorhombic at high temperature (due to the presence of a glide plane in the crystallographic $c$ axis) but develops an increased anisotropy below the onset temperature of a uni-directional CDW state.[31] The specific case of $ErTe_3$ is further discussed below in the context of the present work.

Although the motivation to determine the resistivity anisotropy of orthorhombic materials like those mentioned above is often clear, the quantitative scope of resistivity anisotropy measurements can be significantly restricted by experimental limitations, particularly for small samples. In particular, the absolute magnitude of the anisotropy can be small, especially for temperatures close to a phase transition where the associated order parameter is small. In such cases, one seeks a method that directly measures the resistivity anisotropy, rather than separately measuring the resistivity for different crystallographic directions and taking the difference of these two (typically large) values. In this paper, following a brief introduction to, and appraisal of, conventional techniques, we present a novel approach to directly

[a]Electronic mail: pwalms@stanford.edu

measure the resistivity anisotropy via the transverse resistivity in a rotated experimental frame that addresses some of these limitations without invoking additional assumptions or instrumentation. We frame this discussion in terms of the average and anisotropic contributions to the resistivity, which shows the transverse technique to be less susceptible to the admixture of these quantities. The resistivity anisotropy of the $a$–$c$ plane in $ErTe_3$ is then presented to demonstrate the efficacy of the technique.

## II. METHODS TO MEASURE THE RESISTIVITY ANISOTROPY FOR AN ORTHORHOMBIC MATERIAL

### A. Definition of resistivity anisotropy

In an anisotropic material, the electrical resistivity is described by a second rank tensor $\boldsymbol{\rho}$ that relates the current density $J_j$ to the electric field $E_i$ via the relationship $E_i = \sum_i \rho_{ij} J_j$. When the orientation of the Cartesian basis is defined as parallel to the orthonormal crystallographic axes of the sample ($x \parallel a$, $y \parallel b$, and $z \parallel c$), with some considerations of symmetry, this produces the conventional zero-field resistivity tensor,

$$\boldsymbol{\rho} = \begin{pmatrix} \rho_a & 0 & 0 \\ 0 & \rho_b & 0 \\ 0 & 0 & \rho_c \end{pmatrix}. \quad (1)$$

The resistivity anisotropy is then generally defined as the difference between two given diagonal components ($\rho_{ii} - \rho_{jj}$), although the dimensionless resistivity anisotropies $\frac{\rho_{ii}-\rho_{jj}}{\frac{1}{2}(\rho_{ii}+\rho_{jj})}$ and $\frac{\rho_{ii}}{\rho_{jj}}$ are often more meaningful quantities.

### B. Measurement of resistivity anisotropy by conventional methods

#### 1. Two-bar method

The form of $\boldsymbol{\rho}$ is highly suggestive that the best way to measure ($\rho_{ii} - \rho_{jj}$) is with a current passed, and voltage measured, parallel to the relevant crystallographic axis. Hence the conventional two-bar method, illustrated in Figure 1(a), whereby separate crystals are required to measure each component $\rho_{ii}$ and $\rho_{jj}$. Current and voltage contacts are ideally placed (respectively) on the ends and in the middle of the bar such that current is injected evenly into the sample and the measured voltage represents an average over the orthogonal directions; separation between current and voltage contacts should ideally be at least equal to the width of the bar when considered as an "equivalent isotropic solid" (see Section II B 2) so as to ensure homogeneous current density in the case of uneven contact resistance.

#### 2. Montgomery method

An alternative method to separately determine individual terms in the resistivity tensor was deduced from the earlier work of van der Pauw by Montgomery for anisotropic materials.[32,33] As shown in Figure 1(b), the Montgomery method uses contacts on the corners of a rectilinear sample, through which current is sourced parallel to either planar direction and voltage measured on the parallel opposite pair of contacts. Provided

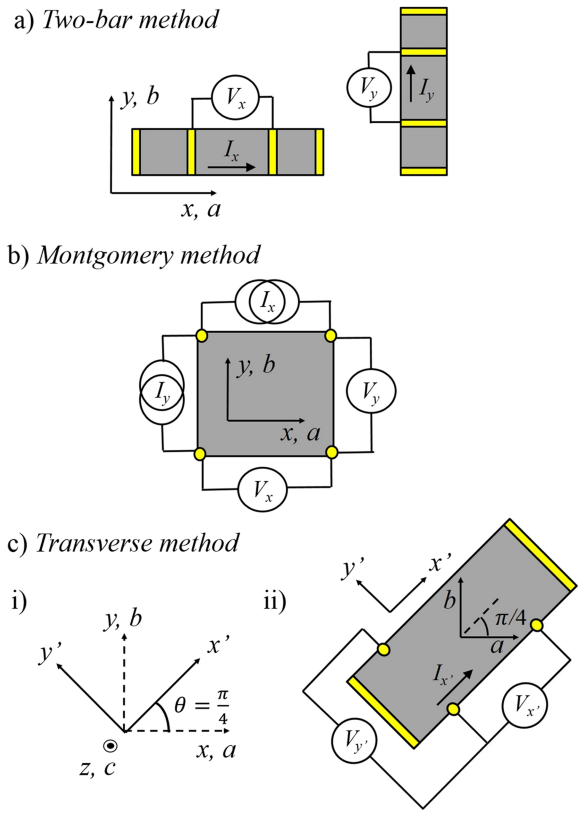


FIG. 1. Schematic diagrams illustrating different methods to determine the resistivity anisotropy of an orthorhombic material. (a) The conventional two-bar method where a separate crystal is used for each component $\rho_{ii}$ to be measured. Any inequivalence between the two measurements or crystals results in admixing of the average resistivity $\frac{1}{2}(\rho_{ii} + \rho_{jj})$ into the inferred resistivity anisotropy ($\rho^m_{ii} - \rho^m_{jj}$), which can affect conclusions drawn about the temperature dependence and magnitude of ($\rho_{ii} - \rho_{jj}$). (b) The Montgomery method uses a single rectilinear sample to measure the resistivity anisotropy with contacts on the corners, currents sourced parallel to the relevant crystallographic direction, and voltage measured across the opposite two corners. This contact geometry produces highly non-linear isopotentials in the sample that typically reduce the magnitude of the measured voltage by an order of magnitude or more relative to the bar method. Geometric factors also non-trivially mix the isotropic resistivity with the inferred resistivity anisotropy. (c-i) The transverse method described in this paper utilises a coordinate system in which the measurement basis is rotated by an angle $\theta = \frac{\pi}{4}$ about the out-of-plane axis (shown here for the case of a rotation about $z$, $c$ for an $a$,$b$ plane anisotropy measurement) to produce a new basis $x'$, $y'$, $z'$ that is no longer aligned to the crystallographic axes $a$, $b$, $c$. As described in the main text, the absence of mirror planes $\sigma_{x'}$ and $\sigma_{y'}$ in this new basis results in finite off-diagonal terms in the resistivity tensor, the values of which are directly proportional to the resistivity anisotropy. (c-ii) The transverse method presented here uses a 5-point contact geometry as illustrated to measure the resistivity anisotropy in a single crystal that has been cut into a bar oriented along the diagonal of the measurement plane (the (110) direction for a measurement of $a$, $b$ plane anisotropy is the example shown here). This geometry does not reduce the magnitude of the voltage signal, and also measures the resistivity anisotropy directly via the transverse contacts (voltage $V_{y'}$ in the illustration), and is less susceptible to admixing of the average resistivity into the resistivity anisotropy.

the sample is close to rectangular with edges well aligned to the crystallographic axes, and its dimensions well known, the measured voltages can be transformed to obtain the resistivity in each crystallographic direction. The first step in this transformation is to consider the theorem employed first by van der Pauw[32] that allows the mapping of an anisotropic solid of any shape to an equivalent isotropic solid; a square of anisotropic material as illustrated in Figure 1(b) maps to a similarly oriented rectangle of isotropic material. The second step is then

to solve the current-voltage relations for this contact geometry in the resultant rectangular equivalent isotropic solid. Simple equations are thus derived that allow intrinsic values of $\rho_{ii}$ and $\rho_{jj}$ to be calculated from the real sample dimensions and the measured resistances.[33] The equivalent isotropic solid is a useful concept more generally in transport measurements, providing an intuitive picture for how electric fields behave in anisotropic systems.

### C. Sources of uncertainty for conventional methods

There is a distinction between how systematic errors affect the absolute value of a single resistivity measurement and the determination of the resistivity anisotropy that varies between methods. The focus here is on minimising the error in $(\rho_{ii} - \rho_{jj})$, as well as considering the errors in $\rho_{ii}$ and $\rho_{jj}$ individually. The following discussion stresses effects that admix the resistivity anisotropy $(\rho_{ii} - \rho_{jj})$ and the average resistivity $\frac{\rho_{ii}+\rho_{jj}}{2}$, noting that these two quantities can have very different temperature dependencies. In particular, as we explain in greater detail below, any technique that aims to measure $(\rho_{ii} - \rho_{jj})$ must minimise admixture of $\frac{\rho_{ii}+\rho_{jj}}{2}$.

#### 1. Two-bar method

In the bar method, the resistivity is derived from the measured resistance $R^m_{ii}$ by geometric factors

$$\rho^m_{ii} = R^m_{ii}\frac{A^m}{l^m}, \tag{2}$$

where $A$ and $l$ are the cross-sectional area of the crystal and the voltage contact separation, respectively, with the superscript $m$ indicating a measured value (as opposed to the intrinsic, error-free values). In principle each of these values has an error associated with its measurement, although the associated uncertainty in $R^m_{ii}$ is generally negligible in comparison to geometric errors and thus omitted from this discussion. $R^m_{ii}$ is however potentially sensitive to crystal misalignment: for a misaligned crystal,

$$R^m_{ii} = [\rho_{ii}\cos^2(\theta) + \rho_{jj}\sin^2(\theta)]\frac{l}{A}, \tag{3}$$

where the misalignment $\theta$ is assumed for simplicity to be solely within the measurement plane, as described by Equation (7). This is generally a reasonable assumption in layered materials. Ideally $\theta = 0$, $l^m = l$, and $A^m = A$, but in any real measurement $\theta = 0 + \Delta\theta$, $l^m = l + \Delta l$, and $A^m = A + \Delta A$. Since misalignment enters $R^m_{ii}$ as $\theta^2$ for small $\theta$, it can be treated as a weak perturbation in most materials and we neglect it here, focusing instead on the more significant geometric factors. In particular, when considering the contribution of geometric errors,

$$\rho^m_{ii} = \rho_{ii}\frac{A^m}{l^m}\frac{l}{A} \approx \rho_{ii}\left(1 + \frac{\Delta A}{A} - \frac{\Delta l}{l}\right), \tag{4}$$

the error in $\rho_{ii}$ is found to be linear in $\Delta A$ and $\Delta l$ and so these errors will dominate. It should be noted however that in the special case of extremely anisotropic materials $(1000\rho_{ii} \approx \rho_{jj})$ contact or crystal misalignment can be the leading error.[34,35] $\Delta A$ and $\Delta l$ can both be large in a single measurement but only appear as multiplicative factors and thus do not affect the temperature dependence of any given component $\rho_{ii}$, thus altering the magnitude but not introducing artifacts. However this situation changes when considering the difference between two components $(\rho_{ii} - \rho_{jj})$. To illustrate this point, we can characterise each measurement as

$$\begin{aligned}\rho^m_{ii} &= \rho_{ii}(1 + \Delta_{ii}),\\ \rho^m_{jj} &= \rho_{jj}(1 + \Delta_{jj}),\end{aligned} \tag{5}$$

and then propagate the measurement errors when finding $\rho_{ii} - \rho_{jj}$,

$$\begin{aligned}\rho^m_{ii} - \rho^m_{jj} = &\frac{1}{2}(2 + \Delta_{ii} + \Delta_{jj})(\rho_{ii} - \rho_{jj})\\ &+\frac{1}{2}(\Delta_{ii} - \Delta_{jj})(\rho_{ii} + \rho_{jj}),\end{aligned} \tag{6}$$

thus showing that terms with different temperature dependences (i.e., $(\rho_{ii} + \rho_{jj})$ and $(\rho_{ii} - \rho_{jj})$) can become admixed. This could fundamentally change the conclusions drawn from an experiment. For example, changes in the average resistivity $(\rho_{ii} + \rho_{jj})$ at a phase transition would lead to an apparent change in the measured anisotropic resistivity $(\rho^m_{ii} - \rho^m_{jj})$, leading to a potentially erroneous conclusion that the phase transition breaks $C_4$ symmetry when in fact it might not.

Whilst the geometric effects are typically the leading error, there are other experimental factors that can lead to an inaccurate determination of $\rho_{ii} - \rho_{jj}$ via the two-bar method; the current density may not be uniform throughout the sample due to poor contact placement, cracks and inhomogeneity in the sample, and deviations from a perfect oblong shape; the two samples used may not be of identical composition or homogeneity, particularly in non-stoichiometric systems; and the temperature measured by the thermometer may not be a perfect representation of the sample temperature. All of these factors will also contribute to the admixing effect discussed above.

The key point from this discussion of the two-bar method is that $(\rho_{ii} - \rho_{jj})$ is highly sensitive to geometric errors and inequivalences in the measurement environment, composition, and contact placement of the two samples. This can be clearly framed in terms of admixing between average and anisotropic components of the resistivity as shown in Equation (6), where it is shown that errors in $\rho_{ii}$ or $\rho_{jj}$ do not just cause an error in the magnitude of $(\rho_{ii} - \rho_{jj})$ but can also give the wrong temperature dependence and the appearance of a significant finite value even for cases where intrinsically $(\rho_{ii} - \rho_{jj}) = 0$ (the case for tetragonal materials). This is particularly acute for the case $(\rho_{ii} - \rho_{jj}) \ll \frac{1}{2}(\rho_{ii} + \rho_{jj})$ (small anisotropies) where the magnitude of the admixing can dwarf the real anisotropy.

#### 2. Montgomery method

The Montgomery method allows for the measurement of $(\rho_{ii} - \rho_{jj})$ in a single sample, with $\rho_{ii}$ and $\rho_{jj}$ measured simultaneously if care is taken over instrumentation.[18] This precludes some of the errors that arise in the two-bar method and has been widely used. There are however some additional considerations arising from the contact and sample geometry (see Figure 1(b)) that should also be considered in the context of the admixing of average and anisotropic resistivities described in Equation (6).

For the Montgomery method to be exactly correct, the sample must be square or rectangular in the plane and of

constant thickness. It has been shown that it is possible to generalise this situation slightly to samples that are parallelograms in the plane and thus only a single additional parameter is required to describe the geometry, but each additional parameter increases the complexity of the analysis, and it may not be possible to solve all situations analytically.[36] The error induced by deviations from the 90° relative angle of the sample edges, $\Delta\phi$, is divergent as angle increases and contributes equally and oppositely to $\rho^m_{ii}$ and $\rho^m_{jj}$. For example, an error of $\Delta\phi = 2°$ gives $\frac{\Delta_{ii}}{\rho_{ii}} = -\frac{\Delta_{jj}}{\rho_{jj}} = 0.01$ with this value increasing to 0.04 for 4°.

The Montgomery method is particularly sensitive to current paths, and as such it is important that the out-of-plane thickness is constant and the sample homogeneous. The magnitude of the thickness is also a non-trivial consideration: the measured voltages have a non-linear relationship with sample thickness as the thickness of the equivalent isotropic solid becomes of the same order as the in-plane dimensions,[33] which can be an issue even in thin samples of highly 2-D materials. The error induced by non-uniform sample thickness is typically of order the proportional change in thickness but can be greater, however, the exact topology of the sample and contact positioning is important and so this error is difficult to treat generally.

Finite contact size is a non-trivial error in the Montgomery technique for the case where the contacts are not negligibly small relative to the sample dimensions. In a bar measurement, using an effective contact centre is a simple solution; however, the same solution applied to the Montgomery method effectively breaks the assumption that the contacts are on the edges of the sample, which is the assumption made in the derivation of the equations used to infer the intrinsic resistivities.

Finally, an important experimental consideration with the Montgomery method is the reduction in the magnitude of the measured voltage due to non-parallel equipotentials produced by the contact geometry (relative to an equivalently sized bar). Typically this reduction can be an order of magnitude in samples with favourable aspect ratios, but becomes far higher as anisotropy increases.[37]

### D. Measurement of resistivity anisotropy by the transverse method

As an alternative to the two-bar and Montgomery methods, we note that the resistivity anisotropy can be accessed directly if we relax the constraint that $a \parallel x$, $b \parallel y$, and $c \parallel z$ under which $\boldsymbol{\rho}$ is conventionally described, and rotate the Cartesian basis (in which the vectors $J_j$ and $E_i$ are defined) relative to the crystallographic axes about the out-of-plane axis by an angle $\theta$ as illustrated in Figure 1(c–i). Assuming anisotropy is to be measured in the $a$, $b$ plane, the conventional resistivity tensor is thus rotated to obtain,

$$R_{z,c}(\theta)\boldsymbol{\rho}R^T_{z,c}(\theta) = \begin{pmatrix} \rho_a\cos^2(\theta) + \rho_b\sin^2(\theta) & (\rho_a - \rho_b)\cos(\theta)\sin(\theta) & 0 \\ (\rho_a - \rho_b)\cos(\theta)\sin(\theta) & \rho_a\sin^2(\theta) + \rho_b\cos^2(\theta) & 0 \\ 0 & 0 & \rho_c \end{pmatrix}, \tag{7}$$

where $R_\alpha$ is the rotation operator about an axis $\alpha$, taken here to be the $z$ and $c$ axes. By setting $\theta = \frac{\pi}{4}$ we obtain

$$\boldsymbol{\rho}' = \frac{1}{2}\begin{pmatrix} \rho_a + \rho_b & \rho_a - \rho_b & 0 \\ \rho_a - \rho_b & \rho_a + \rho_b & 0 \\ 0 & 0 & 2\rho_c \end{pmatrix}, \tag{8}$$

which contains off-diagonal components $\rho'_{x'y'}$ and $\rho'_{y'x'}$ that directly give the in-plane resistivity anisotropy $\frac{\rho_a - \rho_b}{2}$. Herein primed notation indicates the rotated Cartesian basis, thus describing an experiment where $J_{x'}$ represents a current applied at an angle $\theta = \frac{\pi}{4}$ to the $a$ axis and so on. The diagonal components $\rho'_{x'x'}$ and $\rho'_{y'y'}$ give the mean of the in-plane resistivities, $\frac{\rho_a + \rho_b}{2}$. $\rho_a$ and $\rho_b$ can therefore be deduced by combining diagonal and off-diagonal components

$$\begin{aligned} \rho_a &= \rho'_{x'x'} + \rho'_{x'y'}, \\ \rho_b &= \rho'_{x'x'} - \rho'_{x'y'}. \end{aligned} \tag{9}$$

This derivation can be trivially repeated for other measurement planes (indeed in Section III, the measurement is demonstrated in the $a$–$c$ plane for $ErTe_3$). The experimental configuration shown in Figure 1(c–ii) allows the simultaneous measurement of both $\rho'_{x'x'}$ and $\rho'_{x'y'}$ in a single sample. A current is passed along the crystallographic (1 1 0) direction and voltage is measured both parallel and perpendicular to this current. The measured resistances are converted to resistivities in the usual fashion.[38]

The transverse voltage is allowed due to the lack of a mirror plane perpendicular to the $y'$ direction; these mirror planes are necessarily absent in the presence of finite resistivity anisotropy as the resistivity tensor must obey the symmetries of the point group, and no orthorhombic crystal can have diagonal mirror planes. It is important to stress that this measurement scheme is not to be confused with a Hall effect measurement despite the similarities in contact geometry; Hall resistivities are odd under time-reversal and thus zero in the absence of magnetic field or magnetic order in contrast to the present result in Equation (8) which is even under time-reversal. An alternative (but fundamentally equivalent) explanation for the origin of the transverse resistivity in this rotated reference frame is given in Appendix.

### E. Sources of uncertainty for the transverse method

An important experimental concern with the transverse method is that without exceptional care the transverse contacts (nominally measuring $V_{y'}$ in Figure 1(c–ii) will never be truly perpendicular to the current as illustrated in Figure 2. The accidental offset of these contacts lead to a contamination of the transverse voltage characterised by

$$V^m_{y'} = V_{y'} + \frac{l^{y'}_{x'}}{l^{x'}_{x'}}V^m_{x'}, \tag{10}$$

where $V^m_{y'}$ is the voltage measured across the real, misaligned, transverse contacts, $V_{y'}$ the intrinsic transverse voltage, $V^m_{x'}$ the measured longitudinal voltage, $l^{x'}_{x'}$ the measured spacing between the longitudinal voltage contacts, and $l^{y'}_{x'}$ the accidental offset in the $x$ direction of the transverse voltage contacts. If

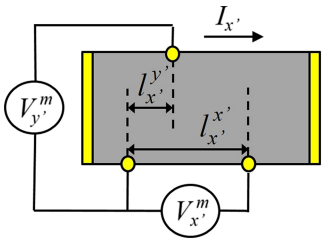


FIG. 2. Unintentional misalignment of transverse contacts in the transverse method causes the measured transverse voltage $V^m_{y'}$ to be contaminated by a longitudinal voltage such that $V^m_{y'} = V_{y'} + (l^{y'}_{x'}/l^{x'}_{x'})V_{x'}$ where $l^{x'}_{x'}$ and $l^{y'}_{x'}$ are the separation in the $x'$ direction of the longitudinal and transverse contacts respectively, as illustrated in the figure ($l^{y'}_{x'}$ is exaggerated for clarity). This accidental misalignment can often be corrected either exactly or approximately when considering the symmetry of the crystal, as described in the main text.

$V_{y'}$ can be assumed to be zero in some regime due to the resistivity being isotropic then Equation (10) allows the determination of $\frac{l^{y'}_{x'}}{l^{x'}_{x'}}$ in this regime. As $\frac{l^{y'}_{x'}}{l^{x'}_{x'}}$ is a temperature independent geometric factor that is constant throughout the measurement, this allows the contamination signal to be subtracted across the whole range of measurement (as $V^m_{x'}$ is also measured). This is not a trivial assumption, but it can be explicitly tested by checking whether $\frac{V^m_{y'}}{V^m_{x'}}$ is constant in the isotropic regime. This condition is perfectly satisfied in the case of a tetragonal to orthorhombic distortion; however, the applicability to the other case discussed in Section I of an orthorhombic material that gains additional anisotropy depends on the specifics of that material. In Section III we argue that the assumption is valid for $ErTe_3$ and its application is demonstrated in Section III C, but this is not a general statement.

The transverse method does not avert errors in sample geometry and finite contact size entirely, but crucially it does eliminate the admixing effects described by Equation (6) when determining $(\rho_{ii} - \rho_{jj})$. The influence of geometric measurement error is now described by,

$$\rho'^{m}_{x'y'} = \rho'_{x'y'}\left(1 + \frac{\Delta A}{A} - \frac{\Delta l^{y'}_{y'}}{l^{y'}_{y'}}\right) = \rho'_{x'y'}(1 + \Delta_{x'y'}), \qquad (11)$$

where $l^{y'}_{y'}$ is the separation in the $y'$ direction of the transverse contacts. Provided the longitudinal contamination signal is correctly subtracted as described above, this shows that geometric errors only manifest as a prefactor to the resistivity anisotropy and do not affect its temperature dependence by admixing the average resistivity $\frac{1}{2}(\rho_{ii} + \rho_{jj})$, in contrast to the two-bar method and Montgomery method. This is a key advantage of the transverse method.

Angular alignment errors are again effectively derived from Equation (7) and contribute to the measurement as

$$\rho'^{m}_{x'y'} = (\rho_a - \rho_b)\cos\left(\frac{\pi}{4} + \Delta\theta\right)\sin\left(\frac{\pi}{4} + \Delta\theta\right), \qquad (12)$$

which is linear in small $\Delta\theta$ but introduces no admixture of $\rho'_{x'x'}$ (inspection of the component $\rho'_{x'y'}$ in the transformed resistivity tensor in Equation (7) makes it clear that angular error does not admix $(\rho_a + \rho_b)$). As with the geometric errors, this gives a prefactor to the resistivity anisotropy without altering the apparent temperature dependence.

For the purpose of geometric error propagation, the measurement of the average resistivity $\rho'_{x'x'}$ can be considered like a single bar method, thus the associated errors are analogous to those described in Equation (4). From Equation (7), misalignment errors give

$$\rho'^{m}_{x'x'} = \rho_a \cos^2\left(\frac{\pi}{4} + \Delta\theta\right) + \rho_b \sin^2\left(\frac{\pi}{4} + \Delta\theta\right), \qquad (13)$$

and it can be seen that $\rho'^{m}_{x'x'}$ becomes weighted towards either $\rho_{ii}$ or $\rho_{jj}$ with finite $\Delta\theta$. As $\frac{d\cos^2(\theta)}{d\theta}$ and $\frac{d\sin^2(\theta)}{d\theta}$ are equal and large in magnitude but opposite in sign around $\theta = \frac{\pi}{4}$, this effect can be appreciable if there is significant anisotropy but largely cancels out in more weakly anisotropic systems.

The error propagation when determining $\rho_a$ and $\rho_b$ individually via Equation (9) using the transverse method is directly analogous to that when determining $(\rho_a - \rho_b)$ via the two-bar method. With reference to Equations (5) and (11), and considering just geometric errors (i.e., neglecting angular misalignment), the values measured by the transverse technique can be written as

$$\begin{aligned}(\rho_a - \rho_b)^m &= (\rho_a - \rho_b)(1 + \Delta_{x'y'}),\\ (\rho_a + \rho_b)^m &= (\rho_a + \rho_b)(1 + \Delta_{x'x'}),\end{aligned} \qquad (14)$$

and thus combine to give

$$\rho^m_a = \rho_a\left(1 - \frac{\Delta_{x'y'}}{2} + \frac{\Delta_{x'x'}}{2}\right) + \rho_b\left(\frac{\Delta_{x'x'}}{2} - \frac{\Delta_{x'y'}}{2}\right), \qquad (15)$$

$$\rho^m_b = \rho_b\left(1 + \frac{\Delta_{x'x'}}{2} + \frac{\Delta_{x'y'}}{2}\right) + \rho_a\left(\frac{\Delta_{x'x'}}{2} - \frac{\Delta_{x'y'}}{2}\right). \qquad (16)$$

Evidently $\rho_a$ can suffer an admixture of $\rho_b$ and vice versa when determined individually via the transverse method, in contrast to the two-bar method where this mixing does not occur. This is analogous to the admixing of $(\rho_a - \rho_b)$ and $(\rho_a + \rho_b)$ in the two-bar method, which does not occur in the transverse method.

Finally, it is important to consider the equivalent isotropic solid in highly anisotropic samples. The sample geometry described in Figure 1(c) maps to a trapezoid for anisotropic materials, and for large anisotropies this may mean that a greater separation between the current and voltage contacts is required for accurate measurements.

In summary, the measurement of $(\rho_{ii} - \rho_{jj})$ by the transverse method is very robust against admixture from the average resistivity, giving a significant improvement on the two-bar and Montgomery methods provided that the contamination signal due to accidental contact offset can be subtracted or minimised. Furthermore, the direct measurement of $(\rho_{ii} - \rho_{jj})$ vastly improves signal to noise by effectively removing the isotropic "background" signal. It is noted that $\frac{\rho_{ii}+\rho_{jj}}{2}$ can become unevenly weighted when measured via the longitudinal contacts due to angular misalignment, but this effect is unlikely to be larger than the contribution of geometric errors in the two-bar method. Measurements of the individual components of the resistivity tensor $\rho^m_a$ and $\rho^m_b$ suffer the effects of admixing between $\rho'_{x'x'}$ and $\rho'_{x'y'}$, and so the transverse method may not offer an improvement over a single bar when

measuring a single component. However, when comparing two components, there is a significant advantage to the transverse method over the two-bar and Montgomery methods, particularly when measuring small anisotropies. This is the principal message of this paper.

## III. DEMONSTRATION OF THE TRANSVERSE METHOD: MEASUREMENT OF RESISTIVITY ANISOTROPY IN $ErTe_3$

### A. Resistivity anisotropy in $ErTe_3$

In order to demonstrate the efficacy of the transverse technique described in the previous section, we have applied the technique to the layered rare-earth tritelluride $ErTe_3$. The rare-earth tritellurides form for $R$ = Y, La-Sm, and Gd-Tm.[40] At high temperature they have the $NdTe_3$ structure type (Cmcm) consisting of RTe blocks separating almost square bilayer Te planes stacked vertically as illustrated in Figure 3. The single layer compound $RTe_2$ has similar motifs ($R$Te block with a single Te layer) and is tetragonal at high temperature. However, $RTe_3$ has a glide plane that causes the material to be very slightly orthorhombic ($a \approx 0.9995c$).[40] Upon cooling, a uni-directional CDW forms along the $c$ direction for all $R$, with heavier $R$ (Tb-Tm) also forming a second CDW along the $a$ direction at lower temperatures. The calculated Fermi surface in the absence of CDW ordering is found to be essentially isotropic in the $a$–$c$ plane (reflecting the almost vanishingly small difference in the $a$ and $c$ lattice parameters), as well as highly two-dimensional, with very little dispersion in the $b$-axis direction.[39] This is because the Fermi surface is almost entirely derived from Te $p_x$ and $p_z$ states in the Te square-net bilayers. Thus in the absence of CDW ordering the material is "almost tetragonal" in the context of electrical transport. The orthorhombicity only becomes a significant factor very close to the CDW transition temperature as phonon frequencies soften in both the $a$ and $c$ directions above the CDW transition temperature $T_{c1}$,[41] but only go to zero in the $c$ direction thus stabilising a mono-domain, uni-directional CDW rather than a bi-directional CDW or domains of perpendicular, uni-direcitonal CDWs. The resultant gapping of the Fermi surface induces significant anisotropy into the electrical transport, thus placing $RTe_3$ into the second category of the material discussed in the Introduction: orthorhombic materials that gain additional anisotropy below some characteristic temperature.[31,42] A crucial advantage with $RTe_3$ over other examples in this class is that the process described in Section II E, whereby longitudinal contamination of the transverse voltage can be subtracted, is applicable owing to the highly isotropic transport properties above $T_{c1}$. This combination of properties make $RTe_3$ the perfect material to demonstrate the efficacy of the transverse method, with the specific example of $ErTe_3$ selected for its convenient CDW ordering temperatures, $T_{c1}$ = 267 K (CDW ordering $\| c$),[40] and $T_{c2}$ = 160 K (CDW ordering $\| a$).[42]

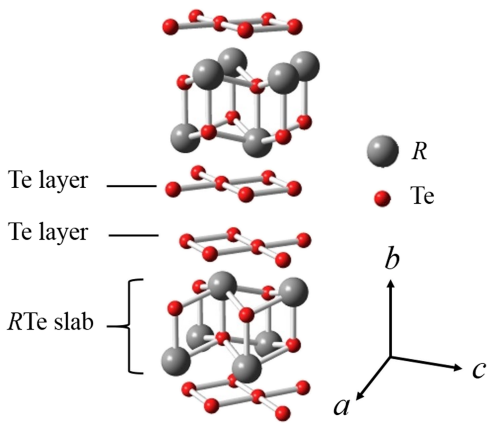


FIG. 3. The structure of $RTe_3$ consists of conducting Te bilayers in the $a$–$c$ plane that are sandwiched between insulating $R$Te slabs. The well separated conducting planes produce a highly two-dimensional Fermi surface that is well described by a simple tight-binding model.[39] As the unit cell is stacked in the $b$ direction, each subsequent unit is offset by half a unit cell in the $a$ direction giving a glide-plane symmetry to the structure. This glide plane is the source of the slight orthorhombicity in the material.

### B. Experimental methods

The experiment was performed using a Quantum Design PPMS temperature controller; voltages were measured via two phase-locked Stanford Research Systems SR830 lock-in amplifiers with current sourced from the reference lock-in's voltage output via a 4.5 kΩ pre-resistor to give a 1 mA current. A nominal gain of 1000 was achieved by combination of a Princeton research model 1900 transformer (100× stepup) and a Stanford Research SR560 pre-amplifier (10× gain) on each voltage channel, and then calibrated. Single crystals of $ErTe_3$ were grown via a self-flux method as described elsewhere,[43] and aligned by x-ray diffraction (via identification of the (0 6 1) peak; (1 6 0) is forbidden in this space group). The sample was cleaved in the $a$–$c$ plane and then cut to produce a bar in the (1 0 1) direction using a scalpel blade, with errors minimised to less than 5° by measuring the angle via an optical microscope in relation to the edges of the as-grown crystal that form in the (1 0 0) and (0 0 1) directions. The cut crystal was 1.4 mm × 0.74 mm × 50 μm in $x$,$z$, and $y$ dimensions. Electrical contacts were made by sputtering gold pads through a mask and then attaching 25 μm gold wires with Dupont 4929N silver paste with the contact geometry illustrated in Figure 1(d). To ensure good contacting on the edges, the sample was inclined and rotated in the sputterer over multiple operations such that the gold pads covered the sides of the sample. Care was taken to ensure that the current contacts fully covered the end of the bar in order to provide a more homogeneous current density. The contacted crystal is shown in Figure 4. Voltage contact separation was measured to the centre of the contacts with the longitudinal contacts separated by 0.49 mm and the transverse contacts separated by 0.64 mm. The contacts were 50–100 μm in size with the offset between the transverse contacts significantly less than the contact size.

### C. Results

Figure 5 shows the measured transverse (blue) and longitudinal (red) voltages ($V^m_{z'}$ and $V^m_{x'}$, respectively). The inset shows that the ratio $\frac{V^m_{z'}}{V^m_{x'}}$ is approximately constant above $T_{c1}$, which by reference to Equation (10) is consistent with almost isotropic in-plane resistivity in the normal state and

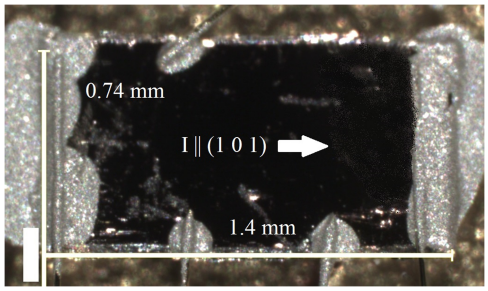


FIG. 4. An optical microscope image of the contacted sample illustrating the contact geometry and finite contact size. The real sample has a gold hue that is not well represented in this image.

a contact offset of 17 μm. The blue dashed line in Figure 5 shows the transverse voltage corrected for this inferred offset, labelled $V_{z'}$. As the offset is a little smaller than the contact size, the error in this correction was estimated by the uncertainty in the position of the effective point contacts, determined optically, with the inferred value found to be within this range. Using these corrected values, the inferred values of $\frac{\rho_a-\rho_c}{2}$ and $\frac{\rho_a+\rho_c}{2}$ are shown in Figure 6(a). Both before and after the subtraction of the contamination signal, the onset of anisotropy below $T_{c1}$ dominates the transverse signal, highlighting the sensitivity of this technique to changes in anisotropy. The dominant error in $\frac{\rho_a+\rho_c}{2}$ is geometric uncertainty due to angular alignment, finite contact sizes, and a relatively thin sample, whereas in $\frac{\rho_a-\rho_c}{2}$ the dominant error is due to the uncertainty in the subtraction of the longitudinal contamination. Note that if $ErTe_3$ were truly tetragonal above $T_{c1}$ then there would be almost no uncertainty in this subtraction.

The resistivities $\rho_a$ and $\rho_c$ were derived via Equation (9) and are plotted in Figure 6(b). Note that no interpolation or fitting was required to add and subtract the data owing to the simultaneous, single crystal measurement. The values

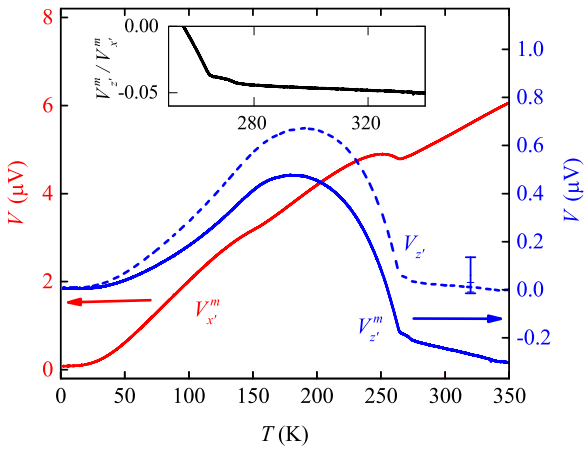


FIG. 5. *Main:* raw voltage data $V^m_{x'}$ (red, left scale) and $V^m_{z'}$ (blue, right scale). Following correction for contact misalignment as described in the main text, $V_{z'}$ is shown as the dashed blue line, with the error bar indicating reasonable uncertainty in the offset of the effective point contacts as determined optically. It is assumed that $V_{x'} = V^m_{x'}$. *Inset:* the ratio $V^m_z/V^m_x$ is shown to be approximately constant above $T_{c1}$, indicating that the in-plane resistivity can be reasonably approximated as isotropic in this region according to Equation (10).

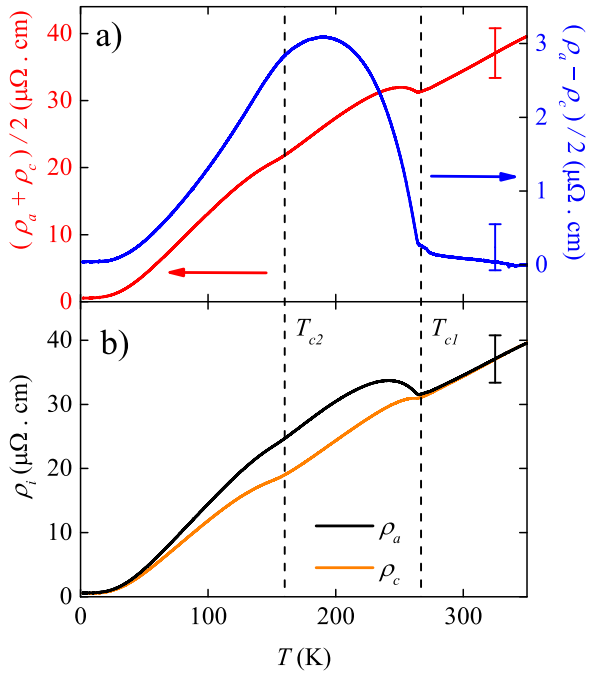


FIG. 6. (a) Average resistivity $\frac{\rho_a+\rho_c}{2}$ (red, left scale) and resistivity anisotropy $\frac{\rho_a-\rho_c}{2}$ (blue, right scale). The error in $\frac{\rho_a+\rho_c}{2}$ is estimated from geometric uncertainties, with the dominant error in $\frac{\rho_a-\rho_c}{2}$ coming from the correction of longitudinal contamination. (b) The calculated values of $\rho_a$ and $\rho_c$ found via Equation (9), the systematic error is dominated by the geometric error in $\frac{\rho_a+\rho_c}{2}$ and is necessarily the same in both $\rho_a$ and $\rho_c$. This data were very well reproduced in a second sample with a different aspect ratio and contact spacing.

obtained are consistent with those found by conventional methods and published elsewhere[31,40,44] and were found to be well reproduced in a second sample with a different aspect ratio and contact separation. The systematic errors are dominated by geometric errors in $\frac{\rho_a+\rho_c}{2}$ that crucially must be identical in the determination of both $\rho_a$ and $\rho_c$.

Two commonly used dimensionless resistivity anisotropies, $\frac{\rho_a-\rho_c}{\frac{1}{2}(\rho_a+\rho_c)}$ and $\frac{\rho_a}{\rho_c}$, are shown in Figures 7(a) and 7(b), respectively; both CDW transitions are easily identified in either plot with the inferred transition temperatures consistent with published values.[40,42] For small deviations from the average, both of these values should have the same temperature dependence, which is consistent with the data. It should be noted that resistivity has a non-trivial relationship to the CDW order parameter, and so $T_{c1}$ indicated in Figures 6 and 7 for comparison is instead taken from x-ray measurements of the associated integrated superlattice peak intensity, with the square root of this value being an appropriate order parameter.[40] An equivalent data set of sufficient quality is not available for $T_{c2}$, and so this was derived from ARPES measurements of the energy gap on the Fermi-surface which should be a good proxy for the order parameter.[42]

## IV. DISCUSSION

The transverse method presented here has a number of advantages over both the two-bar method and the Montgomery method, predominantly because the technique provides a direct

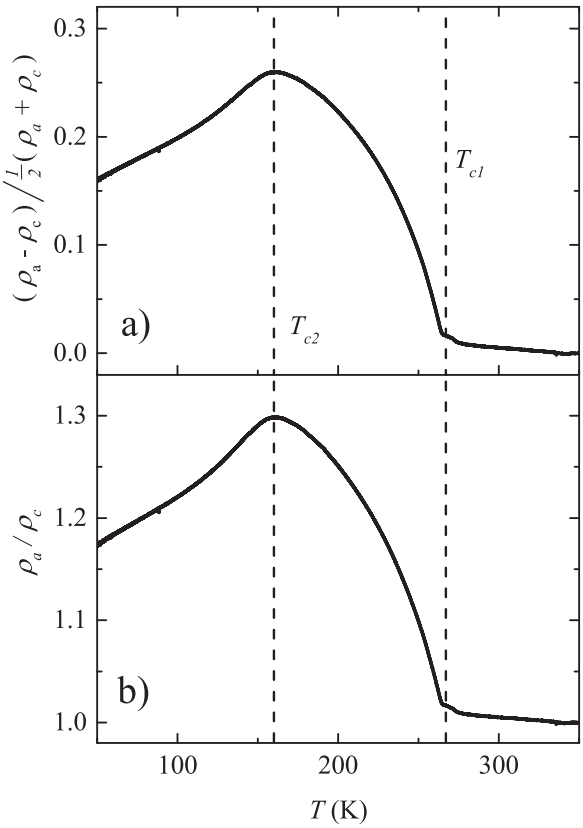


FIG. 7. (a) The dimensionless resistivity anisotropy defined as $\frac{\rho_a-\rho_c}{\frac{1}{2}(\rho_a+\rho_c)}$ shows clear features that coincide with the known transition temperatures $T_{c1}$ and $T_{c2}$ (shown as dashed lines). An alternative dimensionless resistivity anisotropy, $\frac{\rho_a}{\rho_c}$, also highlights very clear features at $T_{c1}$ and $T_{c2}$, as shown in (b). For small deviations from the average value, these two values should have the same temperature dependence, consistent with the data.

measurement of resistivity anisotropy ($\rho_{ii} - \rho_{jj}$) that does not admix with the average resistivity, making it ideally suited for measuring small anisotropies. The present data show clearly how measuring $\rho'_{x'x'} = \frac{\rho_{ii}+\rho_{jj}}{2}$ and $\rho'_{x'y'} = \frac{\rho_{ii}-\rho_{jj}}{2}$ (rather than $\rho_{ii}$ and $\rho_{jj}$ separately) is a useful shift in philosophy that allows greater resolution in both relative and absolute values of ($\rho_{ii} - \rho_{jj}$) whilst still yielding good values of $\rho_{ii}$ and $\rho_{jj}$ individually. The key sources of error with this technique are transverse contact alignment and angular alignment errors in $\rho'_{x'x'}$. The latter is not an issue if ($\rho_{ii} - \rho_{jj}$) is the relevant quantity to be found (because angular misalignment does not admix ($\rho_{ii} + \rho_{jj}$)) and is minimised in absolute terms if $\rho_{ii} \approx \rho_{jj}$. The contribution of the former is robustly corrected for samples that are known to be isotropic in some accessible regime, such as samples undergoing tetragonal to orthorhombic distortions, but requires some caveats in systems which are anisotropic throughout the range of measurement if accurate absolute values are to be obtained. Since $ErTe_3$ is essentially isotropic above $T_{c1}$, this effect is minimised as described above, but this is not generally true for orthorhombic materials. Microlithographic techniques could be employed to minimise the contact offset and angular misalignment in such materials by providing extremely small and well aligned contacts. In general these errors are likely to be less significant than those found in conventional techniques, particularly for small samples. We therefore emphasise that the technique is uniquely sensitive to the resistivity anisotropy in comparison to conventional methods.

Finally, we highlight the critical importance of having a single-domain sample for accurate measurements of the resistivity anisotropy. The presence of domains can create a pseudo-symmetry when averaged over macroscopic length scales that masks the intrinsic anisotropies of the crystal structure, thus leading to an erroneous underestimation, or even elimination, of the resistivity anisotropy. The $ErTe_3$ sample measured here grew as a single-domain, as do many other orthorhombic materials, but this is often not the case. Furthermore, the resistivity anisotropy is often useful in systems that undergo a $C_4$ to $C_2$ rotational symmetry breaking transition, which necessarily forms domains in the absence of an external de-twinning field. It can be possible to de-twin samples *in situ* using, for example, applied magnetic fields[45–48] or strain.[8,9] Ideally this de-twinning field can then be removed below the transition temperature to obtain a single domain in the absence of an applied field,[46] but the sample may simply re-twin depending on the nature of the ordered phase in which case the effect of the detwinning field on the resistivity (the magnetoresistance or elastoresistance in the examples above) must be also accounted for.

## V. CONCLUSIONS

A novel method for measuring the resistivity anisotropy in a single sample utilising transverse resistivity in a rotated experimental frame has been presented and contrasted with conventional methods. It is shown through error propagation that the transverse method is far less susceptible to admixing effects between the anisotropic and isotropic components of the resistivity than conventional methods and thus presents a more accurate measure of the resistivity anisotropy (provided that the transverse contact misalignment is accounted for or minimised as described), particularly for small anisotropies. The technique has been successfully applied to $ErTe_3$, clearly identifying the two CDW transitions from changes in the resistive anisotropy and producing absolute values for $\rho_a$ and $\rho_c$ that are consistent with those already published.[31,40] The direct measurement of ($\rho_a - \rho_c$) via the transverse voltage contacts is shown to be very sensitive to changes in anisotropy. The critical importance of measuring a single-domain sample is also highlighted and discussed. To conclude, in many cases the transverse method should be a substantial improvement on existing methods for measuring resistivity anisotropy in both sensitivity and absolute accuracy.

## ACKNOWLEDGMENTS

The authors would like to thank M. C. Shapiro, S. Aeschlimann, H. J. Silverstein and A. T. Hristov for enlightening and productive discussions. This work was supported by the DOE, Office of Basic Energy Sciences, under Contract No. DEAC02-76SF00515. P.W. was partially supported by the Gordon and Betty Moore Foundation EPiQS Initiative through Grant No. GBMF4414.

## APPENDIX: ALTERNATIVE EXPLANATION OF THE ORIGIN OF THE TRANSVERSE ELECTRIC FIELD

In the transverse technique as applied in the main text to $ErTe_3$, the current is oriented along the (1 0 1) direction, thus the current density $\vec{J}$ vector can be defined as the sum of two vectors aligned to the crystallographic axes, $\vec{J} = \frac{1}{\sqrt{2}}|\vec{J}|(\hat{a} + \hat{c})$. For currents parallel to the crystallographic axes, the conventional resistivity tensor as defined in Equation (1) is appropriate, thus the resultant electric field vector $|\vec{E}|$ becomes,

$$\vec{E} = \frac{1}{\sqrt{2}}|\vec{J}|(\rho_a\hat{a} + \rho_c\hat{c}). \tag{A1}$$

By inspection, $\vec{J} \parallel \vec{E}$ only if $\rho_a = \rho_c$, therefore if the resistivity anisotropy $(\rho_a - \rho_c)$ is non-zero there must be a component of the electric field perpendicular to the applied current. The electric field parallel to the current is found by,

$$\frac{\vec{J}\cdot\vec{E}}{|\vec{J}|} = \frac{1}{2}|\vec{J}|(\rho_a + \rho_c), \tag{A2}$$

and the electric field perpendicular to the current by,

$$\frac{|\vec{J}\times\vec{E}|}{|\vec{J}|} = \frac{1}{2}|\vec{J}|(\rho_a - \rho_c), \tag{A3}$$

where $(\rho_a - \rho_c)$ is the resistivity anisotropy as described in the main text. This approach is also easily generalised for other planes of measurement.


[1] E. Fradkin, S. A. Kivelson, M. J. Lawler, J. P. Eisenstein, and A. P. Mackenzie, Annu. Rev. Condens. Matter Phys. **1**, 153 (2010).
[2] S. A. Kivelson, E. Fradkin, and V. J. Emery, Nature **393**, 550 (1998).
[3] This proportionality is only strictly true in the asymptotic limit, but has been shown to be valid even to large values of the order parameter (see following references).
[4] E. W. Carlson, K. A. Dahmen, E. Fradkin, and S. A. Kivelson, Phys. Rev. Lett. **96**, 097003 (2006).
[5] R. M. Fernandes, E. Abrahams, and J. Schmalian, Phys. Rev. Lett. **107**, 217002 (2011).
[6] E. C. Blomberg, A. Kreyssig, M. A. Tanatar, R. M. Fernandes, M. G. Kim, A. Thaler, J. Schmalian, S. L. Bud'ko, P. C. Canfield, A. I. Goldman, and R. Prozorov, Phys. Rev. B **85**, 144509 (2012).
[7] I. R. Fisher, L. Degiorgi, and Z. X. Shen, Rep. Prog. Phys. **74**, 124506 (2011).
[8] J.-H. Chu, J. G. Analytis, K. De Greve, P. L. McMahon, Z. Islam, Y. Yamamoto, and I. R. Fisher, Science **329**, 824 (2010).
[9] H. Man, X. Lu, J. S. Chen, R. Zhang, W. Zhang, H. Luo, J. Kulda, A. Ivanov, T. Keller, E. Morosan, Q. Si, and P. Dai, Phys. Rev. B **92**, 134521 (2015).
[10] M. A. Tanatar, A. E. Böhmer, E. I. Timmons, M. Schütt, G. Drachuck, V. Taufour, S. L. Bud'ko, P. C. Canfield, R. M. Fernandes, and R. Prozorov, Phys. Rev. Lett. **117**, 127001 (2016).
[11] M. A. Tanatar, E. C. Blomberg, A. Kreyssig, M. G. Kim, N. Ni, A. Thaler, S. L. Budko, P. C. Canfield, A. I. Goldman, I. I. Mazin, and R. Prozorov, Phys. Rev. B **81**, 184508 (2010).
[12] E. C. Blomberg, M. A. Tanatar, A. Kreyssig, N. Ni, A. Thaler, R. Hu, S. L. Bud'ko, P. C. Canfield, A. I. Goldman, and R. Prozorov, Phys. Rev. B **83**, 134505 (2011).
[13] H.-H. Kuo, J.-H. Chu, S. C. Riggs, L. Yu, P. L. McMahon, K. De Greve, Y. Yamamoto, J. G. Analytis, and I. R. Fisher, Phys. Rev. B **84**, 054540 (2011).
[14] T. Liang, M. Nakajima, K. Kihou, Y. Tomioka, T. Ito, C. H. Lee, H. Kito, A. Iyo, H. Eisaki, T. Kakeshita, and S. Uchida, J. Phys. Chem. Solids **72**, 418 (2011).
[15] J. J. Ying, X. F. Wang, T. Wu, Z. J. Xiang, R. H. Liu, Y. J. Yan, A. F. Wang, M. Zhang, G. J. Ye, P. Cheng, J. P. Hu, and X. H. Chen, Phys. Rev. Lett. **107**, 067001 (2011).
[16] J. Jiang, C. He, Y. Zhang, M. Xu, Q. Q. Ge, Z. R. Ye, F. Chen, B. P. Xie, and D. L. Feng, Phys. Rev. B **88**, 115130 (2013).
[17] J.-H. Chu, H.-H. Kuo, J. G. Analytis, and I. R. Fisher, Science **337**, 710 (2012).
[18] H.-H. Kuo, J.-H. Chu, J. C. Palmstrom, S. A. Kivelson, and I. R. Fisher, Science **352**, 958 (2016).
[19] M. D. Watson, T. K. Kim, A. A. Haghighirad, N. R. Davies, A. McCollam, A. Narayanan, S. F. Blake, Y. L. Chen, S. Ghannadzadeh, A. J. Schofield, M. Hoesch, C. Meingast, T. Wolf, and A. I. Coldea, Phys. Rev. B **91**, 155106 (2015).
[20] H.-H. Kuo, M. C. Shapiro, S. C. Riggs, and I. R. Fisher, Phys. Rev. B **88**, 085113 (2013).
[21] H.-H. Kuo and I. R. Fisher, Phys. Rev. Lett. **112**, 227001 (2014).
[22] M. C. Shapiro, A. T. Hristov, J. C. Palmstrom, J.-H. Chu, and I. R. Fisher, Rev. Sci. Instrum. **87**, 063902 (2016).
[23] Y. Gallais, R. M. Fernandes, I. Paul, L. Chauvière, Y.-X. Yang, M.-A. Méasson, M. Cazayous, A. Sacuto, D. Colson, and A. Forget, Phys. Rev. Lett. **111**, 267001 (2013).
[24] A. E. Böhmer, P. Burger, F. Hardy, T. Wolf, P. Schweiss, R. Fromknecht, M. Reinecker, W. Schranz, and C. Meingast, Phys. Rev. Lett. **112**, 047001 (2014).
[25] Y. Ando, K. Segawa, S. Komiya, and A. N. Lavrov, Phys. Rev. Lett. **88**, 137005 (2002).
[26] O. Cyr-Choiniere, G. Grissonnanche, S. Badoux, J. Day, D. Bonn, W. Hardy, R. Liang, N. Doiron-Leyraud, and L. Taillefer, Phys. Rev. B **92**, 224502 (2015).
[27] R. Daou, J. Chang, D. LeBoeuf, O. Cyr-Choiniere, F. Laliberté, N. Doiron-Leyraud, B. J. Ramshaw, R. Liang, D. A. Bonn, W. N. Hardy, and L. Taillefer, Nature **463**, 519 (2010).
[28] J. Chang, N. Doiron-Leyraud, F. Laliberté, R. Daou, D. LeBoeuf, B. J. Ramshaw, R. Liang, D. A. Bonn, W. N. Hardy, C. Proust, I. Sheikin, K. Behnia, and L. Taillefer, Phys. Rev. B **84**, 014507 (2011).
[29] D. Haug, V. Hinkov, Y. Sidis, P. Bourges, N. B. Christensen, A. Ivanov, T. Keller, C. Lin, and B. Keimer, New J. Phys. **12**, 105006 (2010).
[30] J. Chang, E. Blackburn, A. Holmes, N. Christensen, J. Larsen, J. Mesot, R. Liang, D. Bonn, W. Hardy, A. Watenphul *et al.*, Nat. Phys. **8**, 871 (2012).
[31] A. A. Sinchenko, P. D. Grigoriev, P. Lejay, and P. Monceau, Phys. Rev. Lett. **112**, 036601 (2014).
[32] L. van der Pauw, Philips Res. Rep. **13**, 1 (1958).
[33] H. C. Montgomery, J. Appl. Phys. **42**, 2971 (1971).
[34] J.-F. Mercure, A. F. Bangura, X. Xu, N. Wakeham, A. Carrington, P. Walmsley, M. Greenblatt, and N. E. Hussey, Phys. Rev. Lett. **108**, 187003 (2012).
[35] N. E. Hussey, M. N. McBrien, L. Balicas, J. S. Brooks, S. Horii, and H. Ikuta, Phys. Rev. Lett. **89**, 086601 (2002).
[36] K. A. Borup, E. S. Toberer, L. D. Zoltan, G. Nakatsukasa, M. Errico, J.-P. Fleurial, B. B. Iversen, and G. J. Snyder, Rev. Sci. Instrum. **83**, 123902 (2012).
[37] O. Bierwagen, R. Pomraenke, S. Eilers, and W. Masselink, Phys. Rev. B **70**, 165307 (2004).
[38] That is, taking w and d as the width and depth of the sample, $\rho'_{x'x'} = R'_{x'x'}\frac{A_{\perp x'}}{l^{x'}_{x'}} = \frac{V_{x'}}{I_{x'}}\frac{dw}{l^{x'}_{x'}}$ and $\rho'_{x'y'} = R'_{x'y'}d = \frac{V_{y'}}{I_{x'}}d$, provided that the transverse contacts are on the edge of the sample such that $l^{y'}_{y'} = w$. In this case only a single geometric measurement is required for the transverse resistivity, decreasing the associated error contributions. If $l^{y'}_{y'} \neq w$ however then $\rho'_{x'y'} = \frac{V_{y'}}{I_{x'}}\frac{dw}{l^{y'}_{y'}}$.
[39] J. Laverock, S. B. Dugdale, Z. S. Major, M. A. Alam, N. Ru, I. R. Fisher, G. Santi, and E. Bruno, Phys. Rev. B **71**, 085114 (2005).
[40] N. Ru, C. L. Condron, G. Y. Margulis, K. Y. Shin, J. Laverock, S. B. Dugdale, M. F. Toney, and I. R. Fisher, Phys. Rev. B **77**, 035114 (2008).
[41] M. Maschek, S. Rosenkranz, R. Heid, A. H. Said, P. Giraldo-Gallo, I. Fisher, and F. Weber, Phys. Rev. B **91**, 235146 (2015).
[42] R. G. Moore, V. Brouet, R. He, D. H. Lu, N. Ru, J.-H. Chu, I. R. Fisher, and Z.-X. Shen, Phys. Rev. B **81**, 073102 (2010).
[43] N. Ru and I. R. Fisher, Phys. Rev. B **73**, 033101 (2006).
[44] A. A. Sinchenko, P. Lejay, O. Leynaud, and P. Monceau, Phys. Rev. B **93**, 235141 (2016).
[45] J. P. C. Ruff, J.-H. Chu, H.-H. Kuo, R. K. Das, H. Nojiri, I. R. Fisher, and Z. Islam, Phys. Rev. Lett. **109**, 027004 (2012).
[46] S. Zapf, C. Stingl, K. W. Post, J. Maiwald, N. Bach, I. Pietsch, D. Neubauer, A. Löhle, C. Clauss, S. Jiang, H. S. Jeevan, D. N. Basov, P. Gegenwart, and M. Dressel, Phys. Rev. Lett. **113**, 227001 (2014).
[47] Y. Ando, A. N. Lavrov, and S. Komiya, Phys. Rev. Lett. **90**, 247003 (2003).
[48] J.-H. Chu, J. G. Analytis, D. Press, K. De Greve, T. D. Ladd, Y. Yamamoto, and I. R. Fisher, Phys. Rev. B **81**, 214502 (2010).